Martínez-Prieto, LM.; Puche Panadero, M.; Cerezo-Navarrete, C.; Chaudret, B. (2019). Uniform Ru nanoparticles on N-doped graphene for selective hydrogenation of fatty acids to alcohols. Journal of Catalysis. 377:429-437. https://doi.org/10.1016/j.jcat.2019.07.040

Uniform Ru Nanoparticles on N-doped Graphene for Selective Hydrogenation of Fatty Acids to Alcohols

Luis M. Martínez-Prieto,[a] Marta Puche,[a] Christian Cerezo-Navarrete,[a] Bruno Chaudret[b]*

[a] ITQ, Instituto de Tecnología Química, Universitat Politècnica de València (UPV), Av. de los Naranjos S/N 46022, Valencia, España

[b] LPCNO, Laboratoire de Physique et Chimie des Nano-Objets, UMR5215 INSA-CNRS UPS, Institut des Sciences appliquées, 135, Avenue de Rangueil, F-31077 Toulouse, France.

Keywords: Ru nanoparticles • N-doped graphene • Hydrogenation • Fatty acids • Heterolytic hydrogen splitting • Dual-site mechanism

Abstract

Ruthenium nanoparticles (Ru NPs) supported on reduced-graphene oxide doped with N (NH_2-rGO) was synthesized and used for the selective hydrogenation of fatty acids to alcohols, being the hydrogenation of palmitic acid selected as model. Ru was stabilized forming uniform nanometer size particles on N-doped graphene (Ru/NH_2-rGO). The resultant catalyst was very selective for the carbonyl reduction giving 93 % of the aliphatic alcohol at 99 % conversion. The Ru/NH_2-rGO catalysts was more active and selective than the corresponding Ru on non-doped graphene (Ru/rGO) or Ru on carbon (Ru/C). Mechanistic studies points to a dual mechanism for H_2 dissociation, i. e. homolytic and heterolytic cleavage exists on the Ru/NH_2-rGO, while only the homolytic H_2 dissociation occurs on Ru/rGO. This heterolytic splitting, which activates the carbonyl groups and facilitates the hydrogenation of aliphatic acids, is due to the presence of basic centres next to the Ru atoms. The presence of N atoms also increases the stability of the catalyst, allowing a reuse up to four times.

Introduction

The use of biomass and vegetable oils to generate high-value chemicals can contribute to a more sustainable future. In particular, the hydrogenation of fatty acids to alcohols is of great interest for the pharmaceutical and fine-chemical industries.[1] Fatty alcohols are primarily produced by the

petrochemical industry (around 85 % of total production), which is based on non-renewable raw materials.[2] On the other hand, fatty acids, easily obtained from vegetable oils, are starting to be used as low cost renewable resources for the fatty alcohol production. The current industrial process employs Cu-Cr based catalysts under harsh conditions (250-350 °C and 100-200 bar; Scheme 1). It gives relatively low selectivity and suffers important catalyst deactivation.[1a] Recently, several catalysts have been reported for this reaction, and the most active among them operates in homogeneous conditions.[3] Nevertheless, along with the problems of stability and recyclability, they require the addition of a Lewis acid as a promoter, such as $Sn(OTf)_2$, which interacts with the electron pair of the oxygen of the C=O bond, activating it. For the same reason, the majority of heterogeneous catalysts employed in the hydrogenation of fatty acids are bimetallic systems (Ru-Sn, Pt-Re) supported on Al_2O_3 and TiO_2, where the active metal (Ru, Pt) is promoted with a second metal (Sn, Re) that is able to activate the C=O bond.[4] Another way to increase the activity of transition metal catalysts in the selective hydrogenation of the carbonyl groups is the use of reducible oxide supports (TiO_2, MoO_3, ZrO_2, WO_3, etc.), where the oxygen vacancies activate the carbonyl group of the fatty acid. For example, monometallic supported ruthenium catalysts, such as Ru/TiO_2, have shown high activity but low selectivity, producing mostly hydrodeoxygenation products such as alkanes.[5] Taking into account all the above, it would be of much interest to find a stable, selective and active catalyst, able to operate under milder reaction conditions, for the catalytic hydrogenation of fatty acids to alcohols.

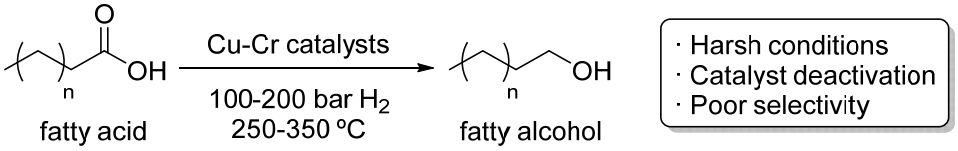

Scheme 1. Industrial production of fatty alcohols from fatty acids.

Metal nano and subnanometric particles, and even isolated single atoms, offer renewed potentiality as catalysts owing to the possibility to modify their electronic properties, allowing to establish a bridge between homogeneous and heterogeneous catalysis.[6] The possibility to support metal nanoparticles (MNPs) on 2D structures such as graphene, that can be functionalized,[7] introduces new possibilities, not only by influencing the electronic properties of the metal, but also by introducing active sites in the

support that can act in a collaborative way with the metal centre. Then, the introduction of functional groups with O, N or P donor atoms affects the metal-graphene interaction, as well as the substrate-graphene interaction. Since MNPs on graphene have demonstrated to be excellent catalysts in many catalytic reactions, including hydrogenation,[8] oxidation,[9] coupling reactions[10] and tandem reactions,[11] the introduction of functional groups in the support can introduce step change in the final catalyst.

It is very well known that hydrogenation of carbonyl groups with supported transition metal catalysts, such as Ru/C, takes place through a homolytic cleavage of the H_2,[12] transferring the chemisorbed hydrogen to the substrate (a of Scheme 2). However, the heterolytic cleavage of H_2 using metal catalysts dispersed on basic supports is an additional possibility for the hydrogenation of carbonyl groups (b of Scheme 2). Indeed, heterolytically dissociated H_2 can be more adequate for the selective reduction of C=O groups. Although the heterolytic splitting of H_2 into H^- and H^+ is not very common on metallic surfaces, it has been previously observed to occur on some catalysts based on MNPs immobilized over basic supports.[13] In the most plausible mechanism, there is not a direct interaction between the substrate and the active metal sites, but the hydrogenation takes place in an outer sphere.[14] Moreover, as this kind of mechanism does not require the direct interaction between the substrate and the metal, it allows to keep the catalyst away from poisoning. Motivated by this novel approach, we decided to immobilize Ru NPs over graphene supports functionalized with N groups, aiming for the generation of bi-functional catalysts constituted by metal particles with adjacent basic surface sites that could also promote the hydrogenation of C=O bonds via heterolytic cleavage.

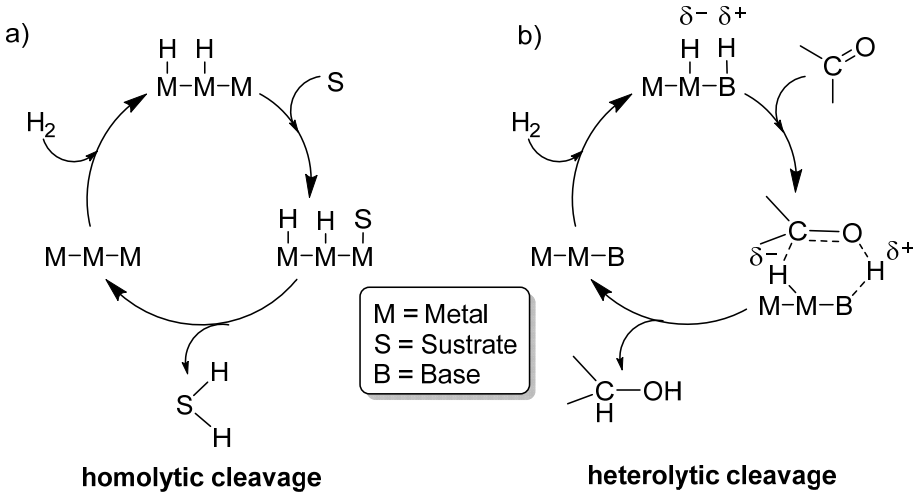

Scheme 2. Hydrogenation mechanisms over solid catalysts.

In most of graphene-supported RuNPs reported until now, $RuCl_3$ was chemically reduced in a solution of GO (Graphene Oxide), leading to the generation of MNPs supported on reduced GO (MNPs/rGO).[7] Here, the reduction of the metallic salt and the support occurs simultaneously with the help of a reducing agent such as $NaBH_4$, hydrazines or amineboranes. On the other hand, the decomposition of high-energy organometallic complexes as a simple route to prepared Ru NPs has been employed for more than 25 years.[15] This organometallic approach protects against potential sources of pollution coming from the reducing agent, or the metal salt used as precursor, since it produces clean surface RuNPs through the decomposition of Ru(cyclooctadiene)(cyclooctatriene) [Ru(COD)(COT)] under dihydrogen in the presence of a stabilizer (ligand, polymer, support, etc.).[16]

Herein, we present for the first time the use of this organometallic approach to synthesize graphene-supported RuNPs with a clean surface and free from polluting residues. To achieve specific metal binding points and the possibility to introduce a second function in the catalyst able to promote the catalysis, a N-doped graphene (NH_2-rGO) was used to support the Ru NPs. For comparison, reduced graphene oxide (rGO) was also used as support (Figure 1). Differences in terms of stabilization, NP dispersion, and catalytic activity were found in both catalysts. The nitrogen atoms in the graphene material contribute to stabilize the Ru NPs by enhancing the interaction MNP-graphene, and also participate in the hydrogenation of carbonyl groups as basic centres. Therefore, the obtained catalytic system (Ru/NH_2-rGO) was used in the hydrogenation of palmitic acid to 1-hexadecanol, and exhibit, as far as we know, a higher activity, selectivity and stability than monometallic Ru heterogeneous catalysts reported so far, without the addition of any promoter.

Results and discussion

1. Synthesis, characterization and surface studies.

Here we have used an organometallic ruthenium precursor and reduced graphene oxide doped and non-doped with N (NH_2-rGO and rGO) to form Ru nanoparticles (Ru/NH_2-rGO and Ru/rGO). More specifically, we decomposed the Ru(COD)(COT) organometallic precursor under H_2 in the presence of the corresponding graphene [room temperature (r.t.), 3 bar H_2, 20h], previously dispersed in THF by

ultra-sonication (Figure 1, top). The metal contents of Ru/NH_2-rGO and Ru/rGO are 2.5 % and 2.4 % by weight, respectively. They were determined by Inductivity-Coupled Plasma Atomic Emission Spectroscopy (ICP-AES) analysis following an optimized digestion method for Ru/C materials (see experimental section, SI).

Transmission electron microscopy (TEM) analysis for Ru/NH_2-rGO revealed spherical, monodispersed and well distributed NPs with a mean diameter of 1.5 ± 0.2 nm (Figure 1a-c). However, when the non-doped rGO was used as support, the size [2.0 ± 0.8 nm] and dispersion of the nanoparticles worsen considerably (Figure 1d-f). This difference in size and dispersion suggests that N atoms present in the N-doped graphene assist the generation and the stabilization of Ru NPs in this synthetic approach. Moreover, we found that for the formation of graphene-supported RuNPs by decomposition of Ru(COD)(COT), it is important to have the graphene in its reduced form, since when we used graphene oxide (GO) as support we could not observe the formation of Ru NPs on the GO sheets (Figure S1, SI). This probably results from the high concentration of oxygenated functional groups at the surface of the graphene, as can be deduced by their elemental analysis (C: 48,2% for GO and C: 83.6% for rGO), which can hinder the interactions between the Ru(COD)(COD) and the graphene material and hence, prevent from the formation of Ru NPs over the oxygenated support. On the other hand, the presence of N atoms in the doped graphenes facilitates this interaction, producing monodisperse and very well distributed MNPs, as observed for Ru/NH_2-rGO.

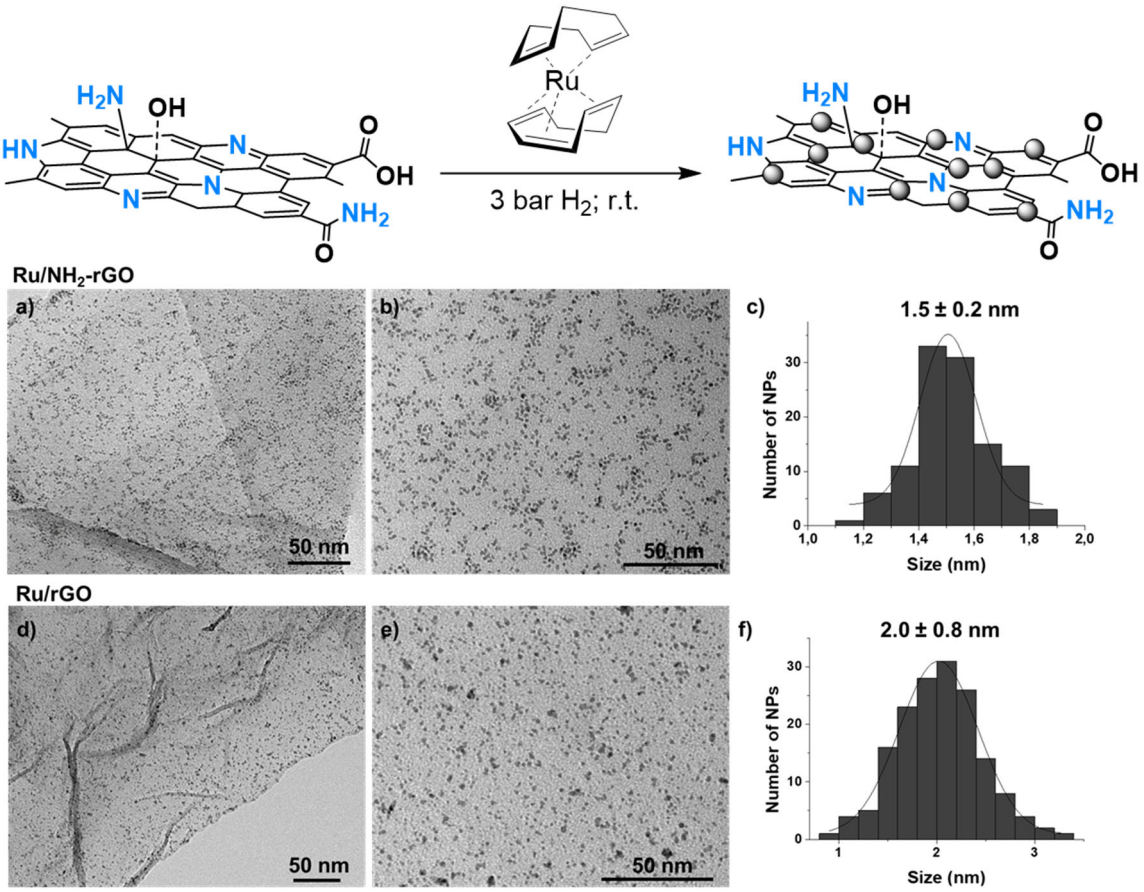

Figure 1. Top: Synthesis of Ru/NH_2-rGO following the organometallic approach. Right: Bottom: TEM images and size distribution histograms of Ru/NH_2-rGO (a- c) and Ru/rGO (d-f).

High-resolution TEM (HRTEM) micrographs of Ru/NH_2-rGO (Figure S2, SI) indicate the existence of crystalline NPs with a hexagonal close packed (hcp) structure for the Ru metal. Fourier analysis applied to these images displays reflections due to the (002), (101) and (002) atomic planes for Ru/NH_2-rGO.

Figure S3 displays X-Ray diffraction (XRD) diffractograms of graphite, GO, NH_2-rGO and Ru/NH_2-rGO. Graphite XRD shows a (002) peak at 2θ = 26.4° corresponding to an interlayer separation of d = 3.36 Å. After oxidation, a new peak appears at 2θ = 11.5° assigned to the (001) plane and corresponding to an interlayer separation of d = 7.64 Å. This large separation between layers is related to the high oxidation degree of the GO. The absence of (002) peak at 24.6° confirms the total oxidation of the graphite. After thermal reduction/exfoliation and NH_3 titration, the peak at 11.5° disappears and a broad peak emerges at 2θ = 24.2°, indicating the reduction of the GO to NH_2-rGO. The XRD pattern for Ru/NH_2-rGO did not present significant differences with the NH_2-rGO one, basically due to the low

metal load (< 3 wt%) and the small size of the NPs that does not allow the observation of the XRD peaks of bulk ruthenium.

As Raman spectroscopy is a well-known characterization technique to evaluate the quality of graphenes,[17] we recorded Raman spectra for NH_2-rGO as well as for their corresponding graphene-supported Ru NPs. The Raman spectrum of NH_2-rGO displays two major bands at 1354 cm^{-1} (D peak) and 1595 cm^{-1} (G peak), together with the 2D´ peak at around 3000 cm^{-1}, which appears very broad (Figure S4a, SI) and is associated to 1-2 graphene layers. The high ratio of the intensities of D and G bands of NH_2-rGO (I_D/I_G = 1.49) and the width of the 2D´ peak are related to the high percentage of defects present in this reduced graphene. These defect sites are exceptional anchoring points for the Ru NPs enhancing the interaction graphene-ruthenium, which may improve the stability and activity of the catalysts. The incorporation of Ru NPs on this material did not affect significantly the Raman spectrum, which mainly showed typical Raman D, G and 2D´ peaks (Figure S4b, SI). Only the I_D/I_G ratio slightly decreased from 1.49 to 1.44, which denotes a larger sp2 domain.[18] In addition, the zoomed region between 200 and 800 cm^{-1} of Ru/NH_2-rGO present small peaks which can be attributed to Ru-C, Ru-N and Ru-O vibrations.

The presence of N atoms and the chemical composition of this N-doped graphene was analyzed by X-ray photoelectron spectroscopy (XPS) (Figure 2). The C 1s signal of NH_2-rGO presents a relative broad band at binding energy (BE) of 284.8 eV, that can be deconvoluted into three components (Figure S5, SI). The main peak at 284.8 eV (pink) is attributed to the carbon atoms of graphitic domains (sp^2). The peak at 286.9 eV (blue) corresponds to carbon atoms of epoxides, tertiary alcohols and C atoms connected to N. The third peak centered at *ca.* 288.8-289.2 eV (red) belongs to carboxylic groups.[19] The N 1s signal of NH_2-rGO, observed at 399.5 eV, is also the result of the convolution of three peaks (Figure 2a). The most intense peak at 399.7 eV corresponds to $–NH_2$ and –NH groups. The peak at 398.6 is characteristic of pyridinic nitrogen atoms and the other one at 401.2 eV belongs to graphitic nitrogen atoms.[20] In conclusion, this study reveals the nature of the different nitrogen-containing groups present in the material, which are doping (graphitic, pyridinic and pyrrolic nitrogens) or functionalizing (amino groups) the rGO surface; the amino and pyrrolic nitrogen atoms being the most abundant. The overlap

of the Ru 3d signal with the C 1s peak (Figure S6, SI), makes the signal deconvolution and interpretation difficult. Therefore, we have studied the different oxidation states of Ru NPs upon analyzing the Ru 3p region. Figure 2b shows the Ru $3p_{3/2}$ signal of the as-synthesized Ru/NH_2-rGO, which displays a binding energy of 462.4 eV. The deconvolution of this peak presents two contributions, one at 463.4 eV that is attributed to Ru(IV), characteristic of RuO_2, and another one at 461.9 eV which belongs to Ru(0).[21] Specifically, the surface of the as-synthesized sample contains 59 % of Ru(IV) and 41% of Ru(0). Interestingly, after heating Ru/NH_2-rGO to 180 °C under H_2 atmosphere during 5 h (close to the catalytic conditions), we were able to reduce the RuO_2 to metallic Ru, observing by XPS an increase of Ru(0) on the surface up to the 72 % (Figure 2c). This suggests that under catalytic conditions (210 °C and 100 bar H_2, *vide infra*) most of the Ru will be in its metallic state, which is the active species in the hydrogenation of C=O groups.

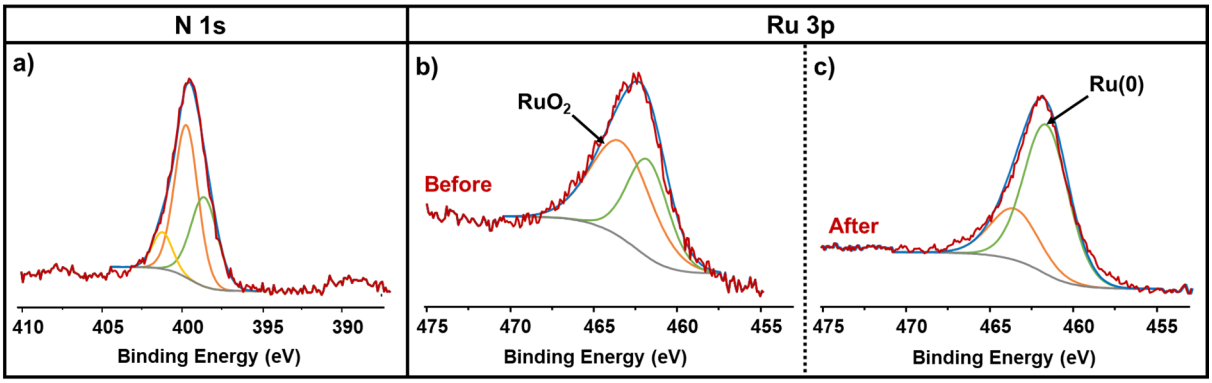

Figure 2. XPS of a) the N 1s signal of NH_2-rGO and the Ru 3p signal of Ru/NH_2-rGO b) before and c) after reduction conditions.

To further study the nature of the N atoms in NH_2-rGO by ^{15}N MAS solid state NMR spectroscopy we synthesized the corresponding doped graphene labelled with ^{15}N ($^{15}NH_2$-rGO). Ammonia-^{15}N was used to prepare it following the same methodology than for NH_2-rGO (for more details see experimental section). ^{15}N MAS NMR spectrum of $^{15}NH_2$-rGO (Figure3, blue) presents a broad band between 330 and 185 ppm, which can be associated to nitrogen atoms that are not close to hydrogen atoms (pyridinic and graphitic N atoms far from H), and a sharper one around 150 ppm, which corresponds to N atoms that are near in space or bonded to H atoms (–NH_2, –NH and graphitic N atoms close to H). This assignation could be clarified from the ^{1}H-^{15}N CP MAS NMR spectrum (Figure 3, orange), where the

intensity of the broad signal between 330-185 ppm is decreased compared to that one at 150 ppm, which means that these N groups are not affected by cross polarization from nearby hydrogen atoms.[22] After the incorporation of Ru to $^{15}NH_2$-rGO (Ru/$^{15}NH_2$-rGO), by employing the aforementioned synthetic method, we obtained Ru NPs with similar size [1.4 ± 0.3 nm], dispersion and distribution than for Ru/NH_2-rGO (Figure S7, SI). No significant differences were observed in ^{15}N MAS and CP-MAS NMR spectra of Ru/$^{15}NH_2$-rGO before and after the incorporation of ruthenium (Figure S8, SI). This is probably due to the enormous width of the peak, where the small chemical displacements corresponding to ^{15}N-Ru interactions (50-70 ppm)[23] are negligible.

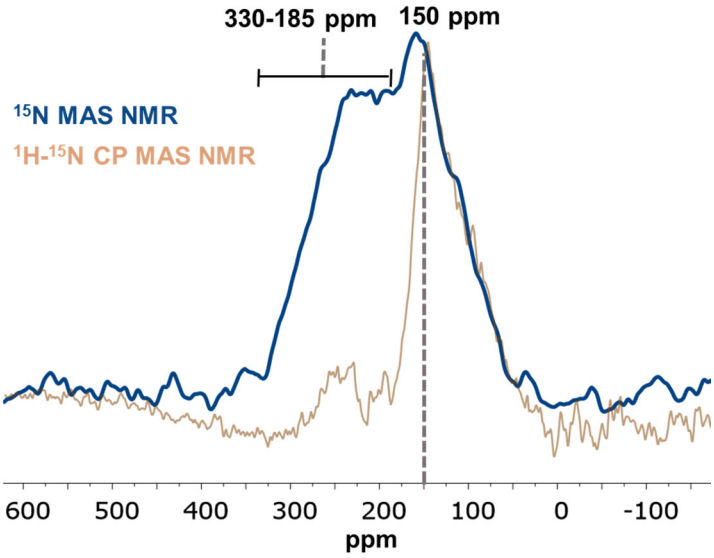

Figure 3. ^{15}N MAS (blue) and CP-MAS (orange) NMR spectra of $^{15}NH_2$-rGO.

Catalytic studies

As mentioned in the introduction, the fatty alcohol production through the hydrogenation of fatty acids is an environmentally friendly process that can be complementary to the industrial one, which is based on petrochemical processes. The hydrogenation of palmitic acid to the corresponding 1-hexadecanol was chosen as a model reaction to measure the activity/selectivity of the catalytic systems prepared. Results of Table 1 show the different products obtained using as catalysts Ru on N-doped and non-doped graphene as well as Ru on carbon at both, high pressure and temperature, in 1,4-dioxane (210 °C and 100 bar). Our initial catalytic experiments started by using Ru/rGO, and by examining selectivity versus

total conversion (Table 1, entry 1), it can be seen that pentadecane **(3)** is also formed, together with small amounts of hexadecane **(4)** and pentadecyl hexadecanoate **(5)**. The formation of 1-hexadecanol **(2)**, via hydrogenation of palmitic acid, is the consequence of a double hydrogenation of the palmitic acid, first to hexadecanal, and after to the corresponding alcohol (Scheme S1, SI). However, three non-desired products can be also be formed: a) pentadecane **(3)**, which is the resulting product of the decarbonylation of 1-hexadecanol,[24] b) hexadecane **(4)**, which comes from the dehydration/hydrogenation of the fatty alcohol, and c) pentadecyl hexadecanoate **(5)**, produced by esterification. The latter can be easily avoided by adding water as co-solvent. The conversion to hexadecane through a hydrodeoxygenation process is very low, but noticeable. The main problem is the decarbonylation of the alcohol, which is difficult to avoid due to the high reactivity of Ru NPs and the harsh conditions necessary to carry out the fatty acid hydrogenation reactions.[25] When the Ru NPs are very active, like in this case, they are able to decarbonylate alcohols, and even other oxygenated solvents, such as THF.[26]

Table 1. Palmitic acid hydrogenation with different Ru catalysts.[a]

Entry	catalyst	Conv (%)[b]	Selectivity (%)[b] 2:3:4:5
1	Ru/rGO	49	86:10:2:2
2	Ru/rGO[d]	24	91:5:2:2
3	Ru/NH_2-rGO	**>99**	**93**:4:2:1
4	Ru/NH_2-rGO (5%)	82	92:4:3:1
5	Ru/NH_2-rGO[e]	59	89:7:3:1
6	Ru/C	17	66:31:2:1

a. Reactions conditions: 0.15 mmol palmitic acid, 25 mg catalyst (~5%, ~ 0.0075 mmol Ru), 10 mL 1,4 dioxane, 0.15 mL H_2O, 100 bar H_2, 210 °C, 22h.
b. Conversions and selectivities were determined by GC using dodecane as internal standard, and confirmed by GC-MS.
c. TOF were calculated taking into account the number of surface atoms, Ru(s). Approximate values obtained from *ChemCatChem* **2011**, *3*, 1413-1418.
d. 1st recycle.
e. Reactions conditions: 0.15 mmol palmitic acid, 25 mg catalyst (~ 0.0075 mmol Ru), 4.8 µL HBF_4, 10 mL 1,4 dioxane, 0.15 mL H_2O, 100 bar H_2, 210 °C, 22h.

Table 1, entry 3 shows that Ru/NH_2-rGO is highly active and gives a remarkable selectivity to 1-hexadecanol. In particular, the conversion was >99 % with 93 % of selectivity towards the corresponding

alcohol with a maximum turn over frequency (TOF) of 3.0 h^{-1} (Table S1, SI). To the best of our knowledge, it presents the best selectivity reported so far by using monometallic Ru heterogeneous catalysts. On the other hand, the larger size and poor dispersion of Ru NPs supported on rGO (Ru/rGO), showed a worse activity and selectivity than Ru/NH_2-rGO (Table 1, entry 1). Finally, and as it was expected, commercial ruthenium catalyst over carbon, Ru/C (5 wt %) showed the worst activity and selectivity for this reaction under our experimental conditions (Table 1, entry 6). In principle, the higher catalytic activity of Ru/NH_2-rGO *Vs* Ru/rGO should be due to the presence of N groups in the graphene sheets, as both supports have a similar exfoliation degree and metal particle size.

To analyse recyclability of Ru/NH_2-rGO, it was reused multiple times. Thus, after a catalytic run, Ru/NH_2-rGO was separated by filtering with hexane and was reused under our standard catalytic conditions (1,4-dioxane, 210 °C, 100 bar H_2, 22h). As shown in Figure 4, both, conversion and selectivity towards 1- hexadecanol were practically preserved during at least four catalytic cycles, observing a slight increase in the selectivity (from 93 to 97 %) and a small decrease in activity (from >99 to 97 %). TEM images of reused Ru/NH_2-rGO, showed a similar Ru distribution on graphene sheets, but the average size [2.6 ± 0.8 nm] and the dispersion of the NPs were presumably higher than before the catalysis (Figure S9, SI). This increase in size and loss in dispersion could be related to the small decrease in activity observed during recycling. On the other hand, after the 1st recycle, the activity of Ru/rGO decreased significantly (Table 1, entry 2). Analysing the TEM pics of Ru/rGO after catalytic conditions (Figure S10, SI), we observed an increment in both, NP size [3.4 ± 1.2 nm] and number of aggregates, what would explain this loss of activity. Therefore, we can assume that the presence of nitrogen atoms holds the particles on the surface and prevents an intensive coalescence.

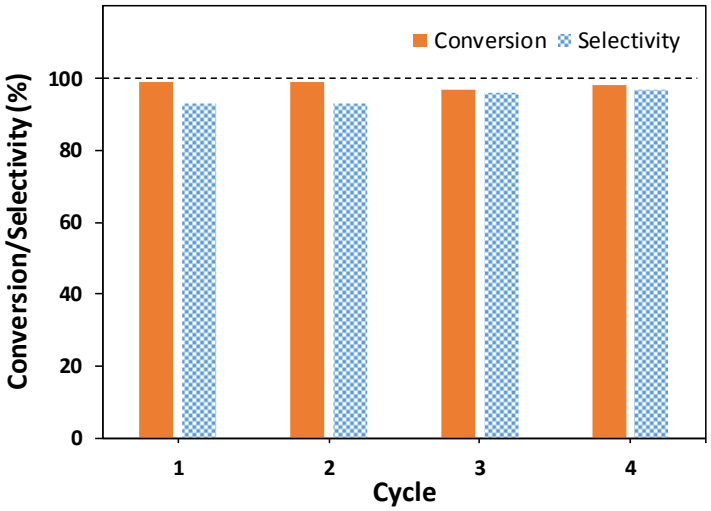

Figure 4. Recyclability experiments of Ru/NH_2-rGO in the hydrogenation of palmitic acid.

The kinetic behaviour of palmitic acid conversion using Ru/NH_2-rGO and Ru/rGO during the first 6-7 h of reaction (Figure 5) shows that the conversion of the palmitic acid practically goes parallel to the formation of the alcohol. Two different conversion rates can be observed within the first hours of reaction. The rate at shorter reaction time is slower and gives a value of 7.8 $mol \cdot h^{-1}$ for Ru/NH_2-rGO and 2.3 $mol \cdot h^{-1}$ for Ru/rGO. This induction period probably is due to time necessary to reduce the remaining RuO_2 to Ru(0) present at the NP surface under catalytic conditions. This is supported by the previous XPS study where the as-synthesized Ru/NH_2-rGO presented 59 % of RuO_2 and 41 % of Ru(0), and after reductions conditions (180 °C under H_2 atmosphere during 5 h) the percentage of Ru(0) on the surface increase up to the 72 %. The latter suggests that under catalytic conditions (210 °C and 100 H_2 bar), almost all the Ru surface is in its metallic state, which is the active species in hydrogenation reactions. The second conversion rate is higher and reaches a value of 13.1 $mol \cdot h^{-1}$ for Ru/NH_2-rGO and 5.3 $mol \cdot h^{-1}$ for Ru/rGO. Small amounts of pentadecane start to appear after 2 hours of reaction using Ru/NH_2-rGO as catalyst or 4 hours with Ru/rGO, in both cases, once the amount of 1-hexadecanol is large enough to experience the decarbonylation process.[24] Something similar happens to the formation of hexadecane, but this secondary reaction occurs even to a lesser extent.

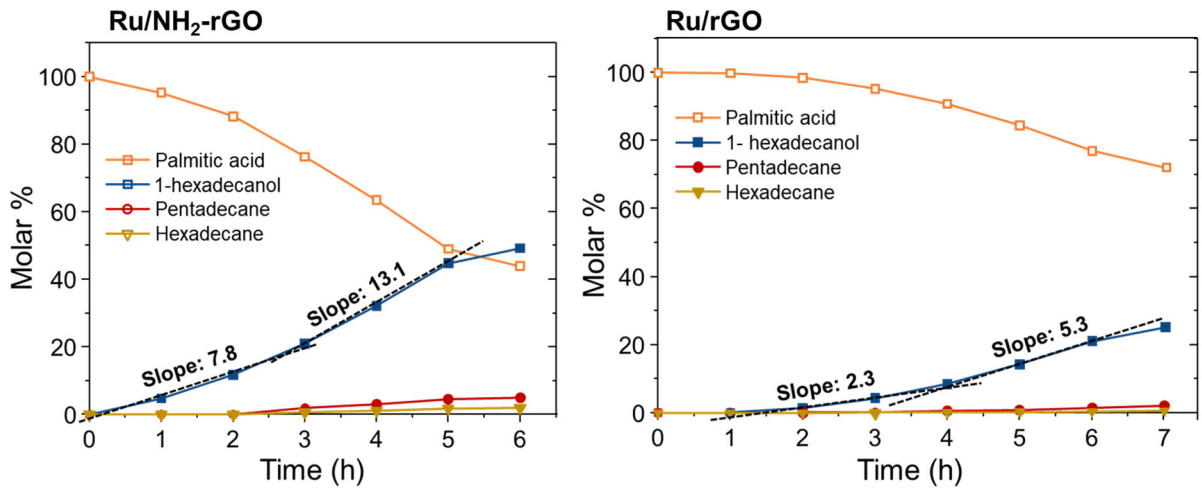

Figure 5. Time course for the formation of 1-hexadecanol using Ru/NH_2-rGO (left) and Ru/rGO (right) as catalyst.

Mechanistic Studies

Since metal content, NPs size and accessible area of Ru/rGO are comparable to those present in Ru/NH_2-rGO, and since the activity of the latter is much higher than Ru/rGO, we can suppose that the presence of the nitrogen in the graphene layer is playing an important role in the catalytic reaction.

To verify the participation of the N atoms in the hydrogenation mechanism, we performed a couple of experiments. First, we prepared Ru/NH_2-rGO but using as support a N-doped graphene with a lower N content (5% instead 8%). The resulting catalyst [Ru/NH_2-rGO (5%)] presents a comparable metal content (2.6 wt % Ru), and the supported NPs have a similar size (1.5 ± 0.3 nm) and size distribution than Ru/NH_2-rGO (Figure S11, SI). However, when we used this catalyst in the palmitic acid hydrogenation reaction under standard conditions, we observed a decrease in the activity but keeping the selectivity (Table 1, entry 4), suggesting that N atoms are involve in the hydrogenation of the carbonyl group. Secondly, we decided to study the kinetic isotope effect of this reaction using Ru/$^{15}NH_2$-rGO. As expected, when the N atoms of Ru/NH_2-rGO were replaced by their corresponding ^{15}N isotopes, the reaction rate was slower. In fact, comparing the time-dependent conversion of palmitic acid using Ru/NH_2-rGO and Ru/$^{15}NH_2$-rGO (Figure S12, SI), we can observe that both, the induction period and the reaction rate (between 3 and 6 h) are lower for Ru/$^{15}NH_2$-rGO than for Ru/NH_2-rGO. The heavier

isotopologues ($^{15}NH_2$ and ^{15}NH) have a minor mobility and an increased stability due to their higher dissociation energy. This kinetic isotope effect reinforces the idea that the N atoms take part in the hydrogenation mechanism.

To corroborate that NH_2 and NH are the N groups that mainly participates in the hydrogenation mechanism, we partially neutralized these basic centres before the catalysis by adding a strong acid with a weakly coordinating conjugate base (HBF_4). Particularly, we added to a typical catalytic reaction 4.8 µL of HBF_4 (0.25 equiv. of H^+ relative to N atoms present in Ru/NH_2-rGO), with the intention to eliminate the basicity of most of the basic centres forming their conjugated acids (NH_3^+ and NH_2^+). As we expected, a considerable reduction of the catalytic activity of Ru/NH_2-rGO occurs and the catalytic conversion is only 59 % (Table 1, entry 5). Therefore, we could confirm that the basicity of the graphene support assists the Ru NPs in the hydrogenation of palmitic acid.

Based on this, two possible mechanisms could explain why the presence of basic centers (-NH_2 and -NH) next to the active metal sites enhances the activity of Ru/NH_2-rGO in the hydrogenation of palmitic acid. A first one, where basic sites are able to deprotonate the palmitic acid forming the corresponding carboxylate, which is subsequently coordinated to the Ru surface (Figure S13, SI),[27] and easily reduced to the corresponding alcohol by an homolytic mechanism (Scheme 2, left). And another plausible mechanism, where two different hydrogenation routes occur at the same time: i) the Ru atoms located in the proximity of the N-doped graphene, are susceptible to split H_2 in a heterolytic way (Site A, Figure 6); ii) in contrast, the other Ru atoms of the particle that are far away from the support, operate as typical metallic sites splitting the H_2 homolytically (Site B, Figure 6). This behaviour has been previously observed in Ru NPs supported on magnesium oxide (MgO), where the surface oxygen atoms act as strongly basic sites.[28]

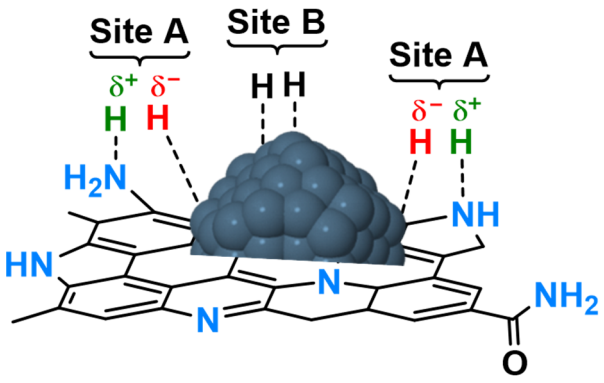

Figure 6. Suggested catalytic sites of Ru/NH_2-rGO for a dual heterolytic/homolytic H_2 splitting.

To shed some light on the operating mechanism we decided to compare the activity of both catalysts (Ru/NH_2-rGO and Ru/rGO) in H/D exchange tests. The isotopic exchange experiments showed that Ru/NH_2-rGO dissociates H_2 faster than Ru/rGO. After a H_2 pre-reduction treatment, the increase of the HD mass signal during H/D exchange experiments at r.t. using Ru/NH_2-rGO and Ru/rGO have a value of 6.64 x 10^{-9} mA and 4.75 x 10^{-9} mA, respectively (Figure S14, SI). The higher rate of Ru/NH_2-rGO in the formation of HD is in favour of the dual heterolytic/homolytic hydrogen cleavage mechanism, where the basic centres of Ru/NH_2-rGO facilitates the dissociation of H_2 in a heterolytic way. Furthermore, the effect of H_2 pressure on the hydrogenation rate was also investigated through a series of kinetic experiments with Ru/NH_2-rGO and Ru/rGO at different pressures (25, 50, 70 and 100 bar). Plotting the hydrogenation rate *vs* H_2 pressure (Figure S15, left), it gives a straight line indicating that the hydrogenation of palmitic acid catalyzed by Ru/NH_2-rGO is highly dependent with respect to the concentration of H_2 (slope: 0.13 $mol \cdot h^{-1} \cdot bar^{-1}$). However, this dependent in much less pronunced for Ru/rGO (slope: 0.06 $mol \cdot h^{-1} \cdot bar^{-1}$; Figure S15, right). This indicates that the palmitic acid hydrogenation is more dependent with respect to the H_2 pressure when we use Ru/NH_2-rGO as catalyst, and also points to the above-mentioned mechanism.

A final experiment that support this heterolytic/homolytic dual mechanism was performed. In detail, we used the hydrogenation of acetophenone as a model reaction to distinguish between the two suggested catalytic sites (A and B). The hydrogenation of acetophenone to 1-cyclohexylethanol can occur through two pathways: path A (blue), where the carbonyl group is hydrogenated in first place to form the 1-phenylethanol, and then the aromatic ring is hydrogenated to form 1-cyclohexylethanol; and path B

(red), where the phenyl group is firstly reduced to the 1-cyclohexylethanone and consecutively the latter is totally reduced to cyclohexylethanol (Figure 7a). We assume that phenyl groups are mostly hydrogenated in Ru faces (site B), whereas carbonyl groups prefer to be hydrogenated by the ionic route (site A). Comparing the initial rates of Ru/NH_2-rGO and Ru/rGO in the hydrogenation of acetophenone, we observed significant differences in their hydrogenation pathways (Figure 7b-c). Ru/NH_2-rGO operates preferable through path A, hydrogenating the carbonyl group much faster than the aromatic ring. Meanwhile with Ru/rGO, the hydrogenation rate of the ketone is slower in comparison with the phenyl group. Indeed, the rate ratio between the formation of 1-phenylethanol and 1-cyclohexylethanone is much higher for Ru/NH_2-rGO (4.50 $mol \cdot min^{-1}$) than for Ru/rGO (3.61 $mol \cdot min^{-1}$). This means that the presence of sites A in Ru/NH_2-rGO boost the hydrogenation of acetophenone through path A, whereas this effect is not so pronounced for Ru/rGO, which mostly present sites B. Therefore, the higher catalytic activity and selectivity of Ru/NH_2-rGO in the hydrogenation of palmitic acid is most likely the result of a dual heterolytic/homolytic hydrogen cleavage mechanism. Otherwise, the Ru/rGO operates by a mechanism in which the homolytic part is the preponderant, and hence, it exhibits a lower catalytic activity/selectivity.

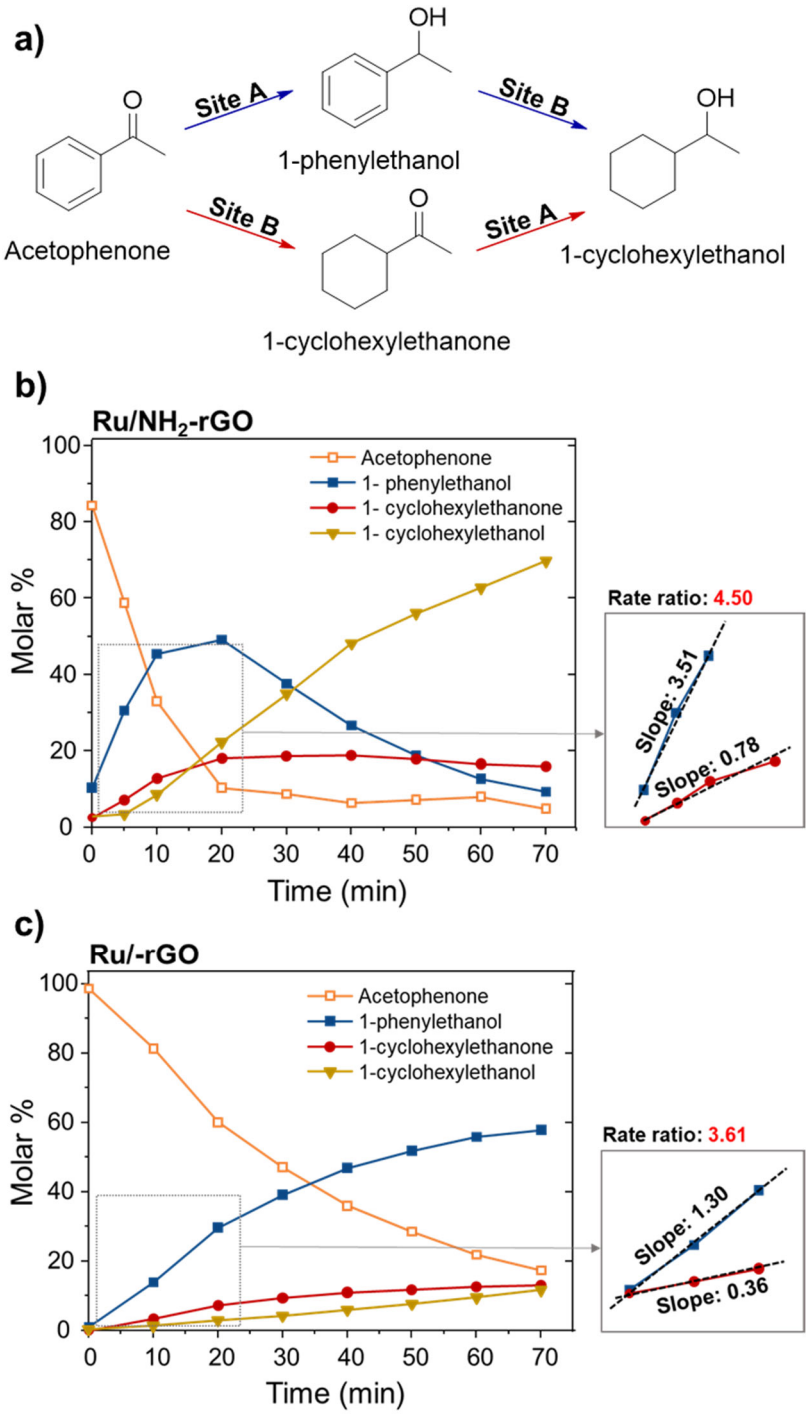

Figure 7. (a) Proposed active sites in the hydrogenation of acetophenone. Time course of the product yield during the hydrogenation of acetophenone using (b) Ru/NH_2-rGO and (c) Ru/rGO as catalyst.

Conclusions

An N-doped graphene-supported Ru NPs (Ru/NH_2-rGO) was prepared, by using for the first time the organometallic approach synthetic method. The presence of N atoms in the graphene material facilitated the generation of small, monodisperse and well distributed NPs. When reduced graphene oxide was

used, the Ru NPs obtained were larger and showed a bad dispersion. The generation of Ru NPs on carbon requires that the surface of the graphene is reduced and is further assisted by the presence of heteroatoms, such as nitrogen. Ru/NH_2-rGO was fully characterized by the state-of-the-art techniques (TEM, HRTEM, XRD, RAMAN and FT-IR). Furthermore, we investigated the presence of the dopant atoms in the graphene and their nature by XPS and ^{15}N solid-state MAS NMR, which are mainly present as amino and pyrrolic nitrogens.

A clear influence of the support was observed on the stability, activity and selectivity in the hydrogenation of palmitic acid into 1-hexadecanol. Ru/NH_2-rGO catalyst showed the best activity and selectivity, because of the presence of basic sites on the support in the proximities of the metal active sites. In this case, the NH_2-rGO not only stabilizes the Ru NPs, but it is also directly involved in the catalytic reactions. This higher activity must be due to the existence of two different hydrogenation pathways operating at the same time, consistent in a dual heterolytic/homolytic H_2 splitting. In contrast, when Ru/rGO was used as catalysts, the predominant operating mechanism was the homolytic cleavage of H_2, what may explain their corresponding lower activity. In addition, the stability of Ru/NH_2-rGO was enhanced by the presence of the nitrogen groups, allowing a reuse up to four times.

To sum up, Ru/NH_2-rGO can be incorporated to a novel family of catalysts that consist of MNPs intimately associated to a basic support, which are not only characterized by their high activity and stability, but also are capable to split the hydrogen in a heterolytic way, increasing their selectivity towards polar C=O bonds.

Acknowledgements

The authors thank Instituto de Tecnología Química (ITQ), Consejo Superior de Investigaciones Científicas (CSIC), Universitat Politècnica de València (UPV) for the facilities. Severo Ochoa excellence programme, "Juan de la Cierva" programme and Primero Proyectos de Investigación (PAID-06-18) for financial support. We gratefully acknowledge Prof. A. Corma for his invaluable contribution to this research. We also thank the Electron Microscopy Service of the UPV for TEM facilities, Jose A. Vidal-Moya (ITQ, CSIC-UPV) for NMR measurements and J. Gaona, and C. Morales for their assistance in catalytic reactions.

References

1. (a) M.A. Sánchez, G.C. Torres, V.A. Mazzieri, C.L. Pieck, Selective hydrogenation of fatty acids and methyl esters of fatty acids to obtain fatty alcohols–a review, J. Chem. Tech. Biotech. 92 (2017) 27-42.; (b) D.S. Thakur, A. Kundu, Catalysts for Fatty Alcohol Production from Renewable Resources, J. Am. Oil Chem. Soc. 2016, 93, 1575-1593.

2. (a) J.V. Gerpen, Biodiesel processing and production, Fuel Process Technol 86 (2005) 1097–1107.; (b) R.G. Herman, Advances in clean fuel technology and control of atmospheric emissions, Catal. Today. 55 (2000) 233–245.

3. (a) T.J. Korstanje, J. Ivar van der Vlugt, C.J. Elsevier, B. de Bruin, Hydrogenation of carboxylic acids with a homogeneous cobalt catalyst, Science 350 (2015) 298-302. (b) X. Cui, Y. Li, C. Topf, K. Junge, M. Beller, Direct Ruthenium-Catalyzed Hydrogenation of Carboxylic Acids to Alcohols, Angew. Chem. Int. ed. 127 (2015) 10742-10745.

4. (a) M. Toba, S.-i. Tanaka, S.-i. Niwa, F. Mizukami, Z. Koppány, L. Guczi, K.-Y. Cheah, T.-S. Tang, Synthesis of alcohols and diols by hydrogenation of carboxylic acids and esters over Ru–Sn–Al_2O_3 catalysts, Tang, App. Catal. A: Gen. 189 (1999) 243-250. (b) H.G. Manyar, C. Paun, R. Pilus, D.W. Rooney, J.M. Thompson, C. Hardacre, Highly selective and efficient hydrogenation of carboxylic acids to alcohols using titania supported Pt catalysts, Chem. Commun. 46 (2010) 6279-6281.

5. L. Di, S. Yao, S. Song, G. Wu, W. Dai, N. Guan, L. Li, Robust ruthenium catalysts for the selective conversion of stearic acid to diesel-range alkanes, App. Catal. B: Environment. 201 (2017) 137-149.

6. (a) L. Liu, A. Corma, Metal Catalysts for Heterogeneous Catalysis: From Single Atoms to Nanoclusters and Nanoparticles, Chem. Rev. 2018, 118, 4981-5079. (b) L. Liu, D.N. Zakharov, R. Arenal, P. Concepcion, E.A. Stach, A. Corma, Evolution and stabilization of subnanometric metal species in confined space by in situ TEM, Nature Commun. 9 (2018) 574. (c) M. Boronat, A. Leyva-Pérez, A. Corma, Theoretical and Experimental Insights into the Origin of the Catalytic Activity of Subnanometric Gold Clusters: Attempts to Predict Reactivity with Clusters and Nanoparticles of Gold, Acc. Chem. Res. 47 (2014) 834-844. (d) M. Flytzani-Stephanopoulos, B.C. Gates, Atomically Dispersed Supported Metal Catalysts, Ann. Rev. Chem. Bio. Eng. 2012, 3, 545-574. (e) A. Corma, Attempts to Fill the Gap Between Enzymatic, Homogeneous, and Heterogeneous Catalysis, Catal. Rev. Sci. Eng. 46 (2004) 369-417.

7. S . Navalon, A. Dhakshinamoorthy, M. Alvaro, H. Garcia, Metal nanoparticles supported on two-dimensional graphenes as heterogeneous catalysts, Coord. Chem. Rev. 312 (2016) 99-148.

8. See for example: (a) M. Gopiraman, S.G. Babu, Z. Khatri, K. Wei, M. Endo, R. Karvembu, I.S. Kim, Facile and homogeneous decoration of RuO2 nanorods on graphene nanoplatelets for transfer

hydrogenation of carbonyl compounds, Catal. Sci. Tech. 3 (2013) 1485-1489. (b) W. Xiao, Z. Sun, S. Chen, H. Zhang, Y. Zhao, C. Huang, Z. Liu, Ionic liquid-stabilized graphene and its use in immobilizing a metal nanocatalyst, RSC Adv. 2 (2012) 8189–8193. (c) R. Nie, J. Wang, L. Wang, Y. Qin, P. Chen, Z. Hou, Platinum supported on reduced graphene oxide as a catalyst for hydrogenation of nitroarenes, Carbon 50 (2012) 586–596.

9. See for example: (a) M. Gopiraman, S. Ganesh Babu, Z. Khatri, W. Kai, Y.A. Kim, M. Endo, R. Karvembu, I.S. Kim, Dry Synthesis of Easily Tunable Nano Ruthenium Supported on Graphene: Novel Nanocatalysts for Aerial Oxidation of Alcohols and Transfer Hydrogenation of Ketones, J. Phys. Chem. C, 117 (2013) 23582–23596. (b) G. Wu, X. Wang, N. Guan, L. Li, Palladium on graphene as efficient catalyst for solvent-free aerobic oxidation of aromatic alcohols: Role of graphene support, Appl. Catal., B: Environ. 136 (2013) 177–185. (c) S. Wu, Q. He, C. Zhou, X. Qi, X. Huang, Z. Yin, Y. Yang, H. Zhang, Synthesis of Fe3O4 and Pt nanoparticles on reduced graphene oxide and their use as a recyclable catalyst, Nanoscale 4 (2012) 2478–2483.

10. See for example: (a) Y. Nishina, J. Miyata, R. Kawai, K. Gotoh, Recyclable Pd–graphene catalyst: mechanistic insights into heterogeneous and homogeneous catalysis, RSC Advances, 2 (2012) 9380-9382. (b) S. Moussa, A.R. Siamaki, B.F. Gupton, M.S. El-Shall, Pd-Partially Reduced Graphene Oxide Catalysts (Pd/PRGO): Laser Synthesis of Pd Nanoparticles Supported on PRGO Nanosheets for Carbon–Carbon Cross Coupling Reactions, ACS Catal. 2 (2012) 145–154. (c) G. Xiang, J. He, T. Li, J. Zhuang, X. Wang, Rapid preparation of noble metal nanocrystalsvia facile coreduction with graphene oxide and their enhanced catalytic properties, Nanoscale 3 (2011) 3737–3742.

11. See for example: (a) H. Göksu, S.F. Ho, Ö. Metin, K. Korkmaz, A. Mendoza Garcia, M.S. Gültekin, S. Sun, Tandem Dehydrogenation of Ammonia Borane and Hydrogenation of Nitro/Nitrile Compounds Catalyzed by Graphene-Supported NiPd Alloy Nanoparticles, ACS Catal. 4 (2014) 1777–1782. (b) C. Su, R. Tandiana, J. Balapanuru, W. Tang, K. Pareek, C.T. Nai, T. Hayashi, K.P. Loh, Tandem Catalysis of Amines Using Porous Graphene Oxide, J. Am. Chem. Soc. 137 (2015) 685–690.

12. G.C. Bond, Metal-Catalysed Reactions of Hydrocarbons, Springer, New York, 2005.

13. (a) R. Juarez, S.F. Parker, P. Concepcion, A. Corma, H. Garcia, Heterolytic and heterotopic dissociation of hydrogen on ceria-supported gold nanoparticles. Combined inelastic neutron scattering and FT-IR spectroscopic study on the nature and reactivity of surface hydrogen species, Chem. Sci. 1 (2010) 731-738. (b) R. Rahi, M. Fang, A. Ahmed, R.A. Sanchez-Delgado, Hydrogenation of quinolines, alkenes, and biodiesel by palladium nanoparticles supported on magnesium oxide, Dalton Trans. 41 (2012) 14490-14497. (c) M. Fang, N. Machalaba, R.A. Sanchez-Delgado, Hydrogenation of arenes and N-heteroaromatic compounds over ruthenium nanoparticles on poly(4-vinylpyridine): a versatile catalyst operating by a substrate-dependent dual site mechanism, Dalton Trans. 40 (2011) 10621-10632.

14. C.A. Sandoval, T. Ohkuma, K. Muñiz, R. Noyori, Mechanism of Asymmetric Hydrogenation of Ketones Catalyzed by BINAP/1,2-Diamine−Ruthenium(II) Complexes, J. Am. Chem. Soc. 125 (2003) 13490-13503.

15. L.M. Martínez-Prieto, B. Chaudret, Organometallic Ruthenium Nanoparticles: Synthesis, Surface Chemistry, and Insights into Ligand Coordination, Acc. Chem. Res. 51 (2018) 376-384.

16. (a) L.M. Martínez-Prieto, S. Carenco, C.H. Wu, E. Bonnefille, S. Axnanda, Z. Liu, P.F. Fazzini, K. Philippot, M. Salmeron, B. Chaudret, Organometallic Ruthenium Nanoparticles as Model Catalysts for CO Hydrogenation: A Nuclear Magnetic Resonance and Ambient-Pressure X-ray Photoelectron Spectroscopy Study, ACS Catalysis 4 (2014) 3160-3168. (b) L.M. Martinez-Prieto, A. Ferry, L. Rakers, C. Richter, P. Lecante, K. Philippot, B. Chaudret, F. Glorius, Long-chain NHC-stabilized RuNPs as versatile catalysts for one-pot oxidation/hydrogenation reactions, Chem. Commun. 52 (2016) 4768-4771. (c) L. Rakers, L.M. Martínez-Prieto, A.M. López-Vinasco, K. Philippot, P.W.N.M. van Leeuwen, B. Chaudret, F. Glorius, Ruthenium nanoparticles ligated by cholesterol-derived NHCs and their application in the hydrogenation of arenes, Chem. Commun., 54 (2018) 7070-7073.

17. R. Saito, M. Hofmann, G. Dresselhaus, A. Jorio, M.S. Dresselhaus, Raman spectroscopy of graphene and carbon nanotubes, Adv. Phys. 60 (2011) 413-550.

18. S. Stankovich, D.A. Dikin, R.D. Piner, K.A. Kohlhaas, A. Kleinhammes, Y. Jia, Y. Wu, S.T. Nguyen, R.S. Ruoff, Synthesis of graphene-based nanosheets via chemical reduction of exfoliated graphite oxide, Carbon, 45 (2007) 1558-1565.

19. *Graphene Oxide: Fundamentals and Applications*, First Edition. Eds: A. M. Dimiev; S. Eigler. 2017 John Wiley & Sons, Ltd. Published 2017 by John Wiley & Sons, Ltd.

20. L. Lai, L. Chen, D. Zhan, L. Sun, J. Liu, S.H. Lim, C.K. Poh, Z. Shen, J. Lin, One-step synthesis of NH2-graphene from in situ graphene-oxide reduction and its improved electrochemical properties, Carbon, 49 (2011) 3250-3257.

21. D.J. Morgan, Resolving ruthenium: XPS studies of common ruthenium materials, Surf. Interf. Anal. 47 (2015) 1072-1079.

22. A.R. MacIntosh, G. Jiang, P. Zamani, Z. Song, A. Riese, K.J. Harris, X. Fu, Z. Chen, X. Sun, G.R. Goward, Phosphorus and Nitrogen Centers in Doped Graphene and Carbon Nanotubes Analyzed through Solid-State NMR, J. Phys. Chem. C, 122 (2018) 6593-6601.

23. P. Leszek, P. Tomasz, S. Jerzy, K. Lech, S. Edward, 1H NMR assignment corrections and 1H, 13C, 15N NMR coordination shifts structural correlations in Fe(II), Ru(II) and Os(II) cationic complexes with 2,2′□bipyridine and 1,10□phenanthroline, Magn. Reson. Chem. 48 (2010) 450-457.

24. A control experiment was carried out to confirm that pentadecane comes from the decarbonylation of 1-hexadecanol (Reactions conditions: 0.15 mmol 1-hexadecanol, 25 mg Ru@NH_2-rGO (~5%, ~ 0.0075 mmol Ru), 10 mL 1,4 dioxane, 0.15 mL H_2O, 100 bar H_2, 210 °C, 22h). For more details, see experimental section part. Furthermore, the palmitic acid hydrogenation at longer conversion time (30 h; Table S1, entry 1) shows how the selectivity toward the pentadecane increases, demonstrating that this byproduct comes from the decarbonylation of 1-hexadecanol.

25. The high temperature and pressure favour the direct decarbonylation versus the dehydrogenation process, which takes place at lower temperature and pressure.

26. (a) P.D. Bolton, M. Grellier, N. Vautravers, L. Vendier, S. Sabo-Etienne, Access to Ruthenium(0) Carbonyl Complexes via Dehydrogenation of a Tricyclopentylphosphine Ligand and Decarbonylation of Alcohols, Organometallics 27 (2008) 5088-5093. (b) S. Mondal, R. Singuru, S. Chandra Shit, T. Hayashi, S. Irle, Y. Hijikata, J. Mondal, A. Bhaumik, Ruthenium Nanoparticle-Decorated Porous Organic Network for Direct Hydrodeoxygenation of Long-Chain Fatty Acids to Alkanes, ACS Sust. Chem. & Engin. 6 (2018) 1610-1619. (c) L.M. Martinez-Prieto, C. Urbaneja, P. Palma, J. Campora, K. Philippot, B. Chaudret, A betaine adduct of N-heterocyclic carbene and carbodiimide, an efficient ligand to produce ultra-small ruthenium nanoparticles, Chem. Commun. 51 (2015) 4647-4650.

27. R. Gonzalez-Gomez, L. Cusinato, C. Bijani, Y. Coppel, P. Lecante, C. Amiens, I. del Rosal, K. Philippot, R. Poteau, Carboxylic acid-capped ruthenium nanoparticles: experimental and theoretical case study with ethanoic acid, Nanoscale, 11 (2019) 9392-9409.

28. M. Fang, R.A. Sánchez-Delgado, Ruthenium nanoparticles supported on magnesium oxide: A versatile and recyclable dual-site catalyst for hydrogenation of mono- and poly-cyclic arenes, N-heteroaromatics, and S-heteroaromatics, J. Catal. 311 (2014) 357-368.